The Diffusion Process of Methane through a Silicalite Single Crystal Membrane

M. Goktug Ahunbay and J. Richard Elliott, Jr.*
Chemical Engineering Department, The University of Akron, Akron, Ohio 44325-3609

Orhan Talu
Chemical Engineering Department, Cleveland State University, Cleveland, Ohio 44115-2425

Received: September 25, 2001; In Final Form: February 25, 2002

The diffusion process of methane in a silicalite single-crystal membrane has been investigated using the Dual Control Volume-Grand Canonical Molecular Dynamics method. Simulations of full-membrane transport and the three individual contributions that comprise the overall process (entrance to the pores, intra-crystalline diffusion, and exit from the pores) show that the contribution of surface resistance to the overall transport resistance in zeolite membranes is larger and longer range than one might expect. A model is proposed on the basis of the additivity of these contributions. From the individual simulations of exit and entrance zones, it is shown that the adsorption and desorption resistances approach an asymptote with increasing crystal thickness. However, the asymptotic trend has not been observed in full membrane simulations within the thickness limit of this work, possibly because of the coupling between the entrance and exit effects. Since the surface resistance is limited to less than 1 μm and the single-crystal membrane comprises 100 μm, the surface resistance still represents a relatively small contribution to the overall resistance. Therefore, the diffusion process through the single-crystal membrane is dominated by the internal transport of the sorbate molecules along the principal (*z*-) axis of the crystal.

1. Introduction

Zeolite membranes combine the general advantages of inorganic membranes (thermal stability, solvent resistance) with perfect shape selectivity, making them versatile adsorbents and specific catalysts. Applications of adsorption cover a wide range of processes from bulk gas separations to purification. Two fundamental aspects control the adsorption process, equilibrium and dynamics. Whereas the equilibrium data in the literature are consistent, the dynamic data, i.e., diffusivities, show variations of several orders of magnitude variations depending on the experimental methods: Quasielastic Neutron Scattering (QENS) and Pulsed-Field Gradient Nuclear Magnetic Resonance (PFG-NMR) (microscopic methods) and zero-length column, frequency response and isotope exchange (macroscopic methods).[1,2] Microscopic techniques involve direct measurement of mobility under equilibrium, whereas macroscopic techniques involve transient measurements. A relatively recent macroscopic technique, single-crystal membrane (SCM) method,[3,4] is based on the direct measurement of diffusive flux through the zeolite at transient and steady-state conditions and allows bridging between the two groups of techniques. The discrepancy between microscopic and macroscopic may be explained in part by the relative contribution of intra-crystalline and inter-crystalline diffusion. Surface resistances (leaving aside the ones due to the preparation process of crystals) exist at the pore entrances and exits due to the discontinuity in the crystal potential field.[5,6] At the continuum scale, Kocirik and co-workers[5] showed that surface resistance can exceed intra-crystalline resistance by several orders of magnitude for crystals smaller than 1 μm. Barrer[7] and Karger[8] developed generalized flux expressions that account for the "evaporation barrier" that arises due to the steep change in potential energy at the zeolite surface.

Entrance and exit barriers are the only existing surface-resistance types in the case of SCM, since the membrane is formed by a single massive zeolite crystal. Therefore, there are only three contributions that comprise the diffusion process of a gas molecule through the SCM: entrance to the pores (adsorption), intra-crystalline diffusion, and exit from the pores (desorption). A number of researchers have studied intra-crystalline diffusion. For example, Maginn et al.,[9] Ford and Heffelfinger,[10] Nicholas et al.,[11] and Hernandez and Catlow[12] investigated the diffusive phenomena of hydrocarbon sorbates inside the zeolite crystal. These studies yielded diffusion-coefficient values in agreement with QENS and PFG-NMR methods.

Entrance into zeolites has been studied by Vigné-Maeder et al.[13] and by Ford and Glandt.[6] The authors investigated the trajectories of gas atoms passing through the outer surface of the crystal. The primary observation from these studies was that entrance into the pore was limited by the ease with which the molecule fit into a pore given its size and conformation.

Arya et al.[14] studied the limiting effect of the pore exit on the transport rate of methane molecules in AlPO4-5-type zeolite. They observed that the surface barrier effect decreases with temperature, and it is more important at sorbate loadings lower than 0.5 molecules per unit cell where the escape of a molecule is unaffected by the presence of the other molecules. At higher sorbate loadings, the local clustering of molecules causes a significant reduction of the pore exit barrier.

Studies of complete membranes have been relatively few and more recent. Takaba et al.[15] studied permeation of iso- and *n*-butane through a 4 nm thick silicalite membrane in the direction of straight channels, showing that the membrane can separate the two isomers. Martin et al.[16] studied the diffusion of methane through silicalite membranes ranging in thickness from 2 to 16 nm, oriented along the straight channels. Their

* Corresponding author. E-mail: jelliott@uakron.edu.

10.1021/jp013613m CCC: $22.00
Published on Web 04/27/2002

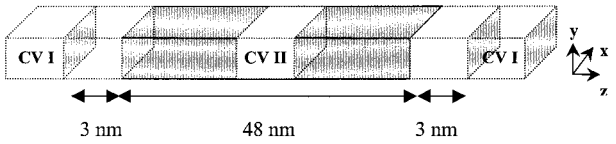

Figure 1. Schematic of DCV-GCMD simulation box. (Not to scale.)

work revealed a strong resistance to flux on both upstream adsorbing surface, and on the downstream desorbing surface.

The objective of this work is to apply Dual Control Volume-Grand Canonical Molecular Dynamics (DCV-GCMD) simulation to understand the dynamics dictating the diffusion of molecules through the SCM, along the *z*-direction. The *z*-direction is the direction in which the SCM is actually operated in practice. Despite these previous works on pore entrance and intra-crystalline diffusion, the pore exit effect has received little attention. In this work, all three effects are analyzed individually as contributions in the sum of mass transfer resistances. Study of these individual steps will help us to better understand the extent of their contribution in different experimental measurement techniques.

In this work, intra-crystalline molecular diffusion is first studied using DCV-GCMD simulation at different operating conditions. Next, the effect of membrane thickness is investigated relative to the contribution of surface resistances with the help of a model based on mass-transfer resistances in series. The study of surface resistance is further extended to individual entrance and exit effects by breaking the simulations down into adsorption and desorption steps.

2. DCV-GCMD Simulations

The basis for DCV-GCMD is to carry out Grand Canonical Monte Carlo (GCMC) insertions and deletions in two control volumes (CVs) placed inside the simulation box of a molecular dynamics simulation (MD), to establish a steady-state chemical potential gradient between these CVs.

The simulation box (Figure 1) consists of two mirror-image boxes, symmetric with respect to the center plane in order to satisfy the periodic boundary condition in the permeating (*z*-)direction. Each symmetric box has three regions: two control volumes CV I and CV II, positioned outside and in the middle of the membrane, respectively, for individual surface studies and a transport region between them. For the intra-crystalline diffusion simulations, both CVs are filled with silicalite, and for the entrance/exit simulations CV II is filled. For total membrane simulations, both CVs are 3 nm away from the corresponding membrane surface.

The chemical potential difference between the CV I and CV II regions acts as the driving force for diffusion of the methane molecules. Therefore the chemical potentials in the two CVs must be maintained at some fixed values, which are in equilibrium with two bulk phases, each at a fixed gas pressure. To keep the densities constant in the CVs, the insertion and destruction algorithms of the GCMC method are implemented. The chemical potentials in the CVs are imposed by the pressure of the gas molecules, under the ideal gas assumption.[17]

$$\beta\mu_{\mathrm{id,gas}} = \beta\mu^{0}_{\mathrm{id,gas}} + \beta \ln\rho \tag{1}$$

and

$$\beta\mu^{0}_{\mathrm{id,gas}} = \ln \Lambda^{3} \tag{2}$$

where Λ is the de Broglie wavelength. Equation 1 can be rewritten in terms of the ideal gas pressure $P_{\mathrm{id,gas}}$,

$$\beta\mu_{\mathrm{id,gas}} = \beta\mu^{0}_{\mathrm{id,gas}} + \beta \ln \beta P_{\mathrm{id,gas}} \tag{3}$$

Thus the probability of inserting a particle is given by

$$p^{+} = \min\left[1, \frac{V\beta P_{\mathrm{gas}}}{(N+1)} \exp\{-\beta\Delta U\}\right] \tag{4}$$

where V is the volume of the CV I or CV II, and P_{gas} is the pressure of the gas bath, which is in equilibrium with the corresponding CV. Similarly, the probability of deleting a particle is given by

$$p^{-} = \min\left[1, \frac{N}{V\beta P_{\mathrm{gas}}} \exp\{-\beta\Delta U\}\right] \tag{5}$$

When a particle is inserted in a CV, it is assigned a random thermal velocity selected from a Gaussian distribution at the given temperature. A streaming velocity was added to the thermal velocity of all the newly inserted methane molecules that were located within 1 nm of the boundaries in each CV, to maintain continuous and monotonic chemical potentials at the boundaries between the CVs and the transport region.[18] Addition of streaming velocities was also necessary to prevent backward convective flux developing in the transport regions.[19] The magnitude of streaming velocity was set by a trial and error procedure as such that the chemical potential be constant inside the control volumes and no discontinuity occur at the boundaries of the control volumes. The final increment in velocity of the *z*-component was roughly 60 m/s within the 1 nm regions at the cell boundaries. Note that the method of setting the streaming velocity within a narrow region of the control volume[18] is different from setting it over the entire control volume,[19] so the exact settings may vary, depending on the method of application.

Molecules spontaneously move along the chemical potential gradient through a conventional molecular dynamics algorithm, and a nonequilibrium steady state is obtained in the transport region. A 5.0 fs MD-time step was adopted and the simulations were run for 100 to 200 ns. Isothermal conditions were maintained by rescaling the velocity in all three directions. To maintain the correct density and chemical potentials in the CVs, the ratio of GCMC steps to MD steps was set at 1:100 for CV I, and varied between 1:200 and 1:500 for CV II.

To obtain the chemical potential profile, the membrane was divided into bins and the excess chemical potential within these bins was calculated by the test particle insertion method of Widom.[17]

$$\mu = \mu_{\mathrm{id,gas}} + \mu_{\mathrm{excess}} \tag{6}$$

In the present work, the spherical Lennard-Jones (LJ) potential model was used for the CH_4 molecules and methane−zeolite interactions. The silicalite framework is assumed to be rigid. The silicon atoms in the zeolite were neglected and, to account for their absence, modified oxygen interaction parameters were used. All interactions of $CH_4 - CH_4$ and $CH_4 - O$ atoms were described by the 12-6 LJ potential given as

$$\phi_{\mathrm{ij}} = 4\epsilon_{\mathrm{ij}}\left[\left(\frac{\sigma_{\mathrm{ij}}}{r}\right)^{12} - \left(\frac{\sigma_{\mathrm{ij}}}{r}\right)^{6}\right] \tag{7}$$

where r is the distance between interaction centers, i and j, which are allotted among CH_4 molecules or oxygen atoms, and σ_{ij} and ϵ_{ij} are potential parameters for the pair i and j. The pure LJ parameters for the CH_4 ($\sigma_{CH_4} = 0.373$ nm, $\epsilon_{CH_4}/k_B = 148$ K) were taken from Vlugt et al.,[20] and those for the methane−

zeolite interactions ($\sigma_{CH_4} = 0.364$ nm, $\epsilon_{CH_4-O}/k_B = 96.5$ K) were taken from the work of Smit and Siepmann.[21] The cutoff distance for calculations of the intermolecular interactions was set at 1.0 nm, and the long-range correction was not applied. The potential and the force vector were evaluated using the pretabulation method, which uses the symmetry property of the 1/8th zeolite unit cell.[22,23]

3. Results

To evaluate individual contributions of adsorption, intra-crystalline transport, and desorption steps into the diffusion process and to avoid any coupling effect between entrance and exit effects, the simulations for each operating conditions were broken down to three regions: entrance, intra-crystalline, and exit simulations. The flux during an intra-crystalline simulation is given by

$$j = -\frac{D_t \Delta P}{RT \Delta z} = -\frac{D_t}{RT}\frac{\Delta P}{L} \tag{8}$$

where D_t is uncorrected transport diffusivity. This flux can be rewritten in terms of a diffusive resistance as:

$$j = -\frac{1}{R_{intra}}\frac{\Delta P}{RT} \tag{9}$$

Similarly, the total resistance acting on a complete membrane may be calculated as the sum of individual contributions,

$$R_{tot} = R_{ads} + R_{intra} + R_{des} \tag{10}$$

where R_{ads} and R_{des} are the resistances to adsorption and desorption. The overall flux is related to the total pressure of the system by

$$J_o = -\frac{1}{R_{tot}}\frac{\Delta P}{RT} \tag{11}$$

Then the overall diffusion coefficient as measured experimentally can be represented as

$$D_{exp} = \frac{L}{\left[R_{ads} + \frac{L_{intra}}{D_t} + R_{des}\right]} \tag{12}$$

One question addressed by the simulations is whether the surface resistances are substantial enough to alter the value of D_{exp}, or whether $D_{exp} \sim D_t$ is a reasonable approximation. During the calculations, we observed that the fugacity became relatively flat at short distances from the surface. Hence, L_{intra} was set to equal to L, the distance between the crystal surface and CV II, to simplify the analysis.

3.1. Intra-crystalline Resistance. Intra-crystalline simulations were conducted by creating a pressure/fugacity gradient inside the crystal as described in the previous section. These simulations have revealed the isolated contribution of the intra-crystalline transport. The thickness of the crystal was varied from 24 to 48 nm to check any possible bias that was created by the distance between two control volumes.

Since the transport diffusivities vary with concentration,[1] the corrected diffusivities D_o were calculated using Darken's correction factor[4] to account for the effect of operating pressure in the CVs:

$$D_o = D_t\frac{d \ln q}{d \ln P} \tag{13}$$

where q is the concentration in the micropores. Thermodynamic definitions provide a link between the concentration and the surface excess amount absorbed n:

$$q = n\rho_s + \epsilon\rho_g \tag{14}$$

where ρ_s and ρ_g are the crystal and gas densities, respectively, and ϵ is the microporosity. After some mathematical manipulation, corrected diffusivity can be defined as

$$D_o = \frac{J_o.L}{\rho_s.\Delta\psi + \epsilon.\frac{\Delta P}{RT}} \tag{15}$$

The spreading pressure difference ($\Delta\psi$) between the entrance and the exit is calculated by integrating

$$d\psi = n(d \ln P) \tag{16}$$

A virial isotherm equation is used to relate n to P. The details of the calculation are given elsewhere.[4] The corrected diffusivities calculated by eq 15 are listed in Table 1 along with the transport diffusivities. The table also includes the simulation parameters.The results are compared with previous in Figure 2. The corrected diffusivities obtained in this work agree qualitatively with the experimental data[4] and with the results of previous works.

3.2. Membrane Simulation. The contribution of surface resistance with increasing membrane thickness has been investigated by varying the thickness from 16 to 64 nm. The temperature of the system was kept at 298 K, and the inlet pressure was set to 1 bar. Simulation runs were carried out for the outlet pressure at vacuum. Surface resistance for the membrane was calculated by subtracting intra-crystalline resistance from total resistance:

$$R_{surf} = R_{tot} - R_{intra} \tag{17}$$

Results of these simulations indicate that the surface resistance along the membrane increases linearly with the membrane thickness in the range studied as presented in Figure 3. This finding calls into question the assumption that the surface resistance is constant for sufficiently long membranes, making intra-crystalline diffusion the only significant resistance. Note, however, that the error bars in the estimated surface resistance become large for thicker membranes. This occurs because the subtraction in eq 17 results in a small difference between large numbers as the membrane becomes thicker and because the maintenance of steady state occurs for a smaller proportion of the total simulation time for the thicker membranes. For the thickest membranes, where the internal loading was roughly 1 molecules/unit cell, steady state was indicated after 1000 ns of simulated time, corresponding to 3−4 weeks of continuous computer simulation on an 800 MHz Pentium III processor.

The dependence of surface resistance on membrane thickness has also been observed by Martin et al.[16] In their work, where they studied the diffusion of methane along the straight channels of silicalite, an alternative approach was used to model the membrane permeation, on the basis of the assumption that the adsorption and desorption resistances were equal:

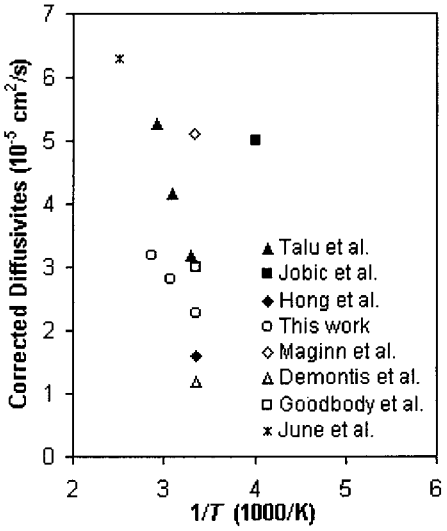

Figure 2. Comparison of corrected diffusivities with previous works given in ref 4. Solid marks represent experimental works, and hollow marks represent simulation results.

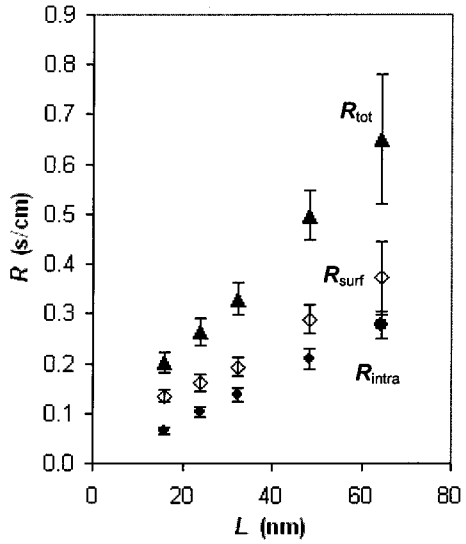

Figure 3. Change of mass-transfer resistances with membrane thickness. Error bars indicate standard deviations of flux values (10% except that of 4*L*, which is 20%).

$$J = \frac{(p_{in} - a\exp(\beta\mu_{ads}))}{R_{ads}RT} = \frac{c_m\beta(\mu_{ads} - \mu_{des})}{R_{intra}RT} = \frac{(a\exp(\beta\mu_{des}) - p_{out})}{R_{des}RT} \quad (18)$$

where c_m is the intra-crystalline sorbate concentration, and since $R_{ads} = R_{des}$,

$$\frac{B_{surf}}{RT} = \frac{1}{R_{surf}RT} = \frac{J[1 + \exp(JL_{intra}/D_o c_m)]}{P_{in} - P_{out}\exp(JL_{intra}/D_o c_m)}, \quad (19)$$

where B_{surf} is the surface-mass-transfer coefficient ($B_{surf} = 1/R_{surf}$). They reported that B_{surf} decreased (thus the surface resistance increased) with the length of the membrane. To compare the results of both works, their original mass-transfer coefficients were corrected by Darken's factor. Table 2 shows original and corrected mass-transfer coefficients and surface resistance. The linear increase in surface resistance can be seen in Figure 4.

TABLE 1: Intra-crystalline Transport and Corrected Diffusivities of Methane

T (K)	P_{in} (kPa)	P_{out} (kPa)	L (nm)	j_{intra} (mol/m^2 s)	D_o (10^{-5} cm^2/s)	D_t (10^{-5} cm^2/s)
298	100	0	16.11	198.8	2.24	7.93
298	100	0	24.17	133.9	2.26	8.02
298	100	0	32.22	103.0	2.32	8.22
298	50	0	16.11	102.0	2.20	8.14
298	250	100	16.11	225.0	2.33	5.99
298	300	100	16.11	274.3	2.26	5.47
298	350	100	16.11	320.9	2.23	5.12
325	100	0	16.11	124.1	2.71	5.40
350	100	0	16.11	85.1	3.16	3.99
350	300	100	16.11	163.0	3.30	3.82
350	100	0	32.22	42.3	3.14	3.97

TABLE 2: Results from the Work of Martin et Al.[a,b]

L (nm)	B_{surf} (m/s)	R_{surf} (s/m 10^{-2})	$R_{surf,\,corr}$ (s/m)
2	26.5	3.8	1.9
4	23.4	4.3	2.1
8	21.4	4.7	2.3
16	17.0	5.9	2.9

[a] Ref 16. [b] Where B_{surf} is the mass-transfer coefficient reported in the original work, the corresponding surface resistance (R_{surf}) is further corrected using Darken's factor ($R_{surf,corr}$).

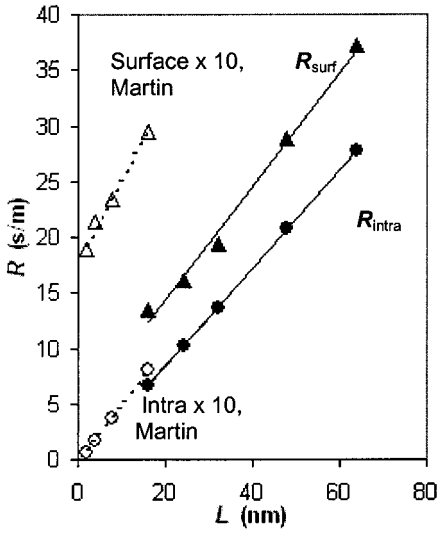

Figure 4. Linear increase in surface resistance calculated by Martin et al.[16] (hollow marks) in comparison with this work (solid marks). Since the resistances calculated by the authors are in the *y*-direction, they are smaller than those of in *z*-direction.

This unexpected behavior might be attributed to the artificially large pressure gradients along a relatively thin membrane. In experimental works the pressure gradients were around 20 Torr along 100 μm and the drops in chemical potential at the surfaces must be much smaller than observed in the present simulations. Further work with thicker membranes under small potential gradients would unveil the effect of the pressure gradient, but would require more advanced computational resources in order to be feasible. The computational cost for membrane simulations increases linearly with crystal thickness, as a longer sampling time is required to avoid temporal fluctuation of gas flux along the membrane, and as the simulated time to achieve steady-state conditions increases. The thickest membrane studied in this work had a thickness of 64.5 nm. Figure 5 shows the time-dependent distribution of fluxes calculated at 5 equidistant points between the entrance and exit of membrane. Another potential explanation could relate to the assumption of fixed atom

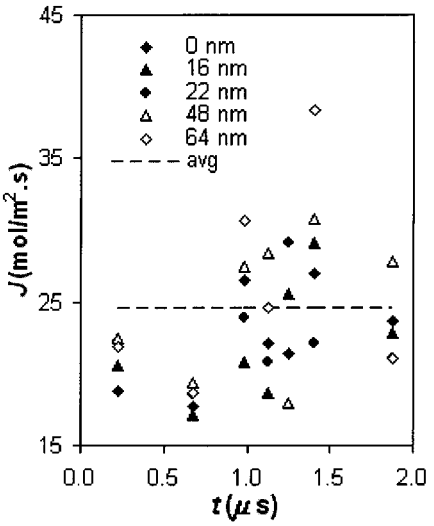

Figure 5. Temporal fluctuation of methane flux through the membrane 4*L*. The first two sets of data were discarded and sampling was started after 1 μs.

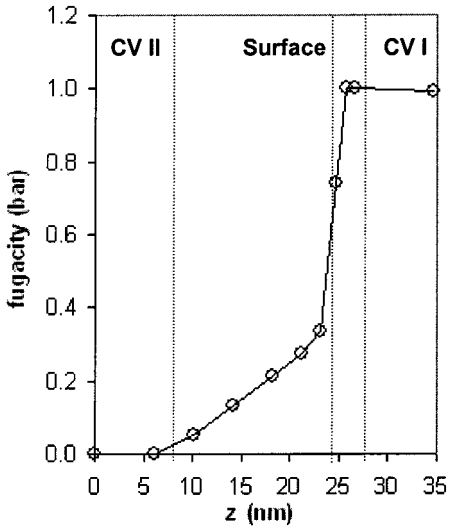

Figure 6. Fugacity gradient for the entrance step: CV I and CV II are at 1 bar and vacuum, respectively.

positions for the crystal, assumed in order to permit pretabulation. This assumption might cause the energies of gas atoms to be correlated over longer distances since the solid atoms cannot dissipate gas−gas influences. On the other hand, the dependence of the surface resistance on membrane thickness may be a realistic aspect of the simulation. To begin with, there is the edge effect of the potential from the solid, but the range of this effect is roughly reflected by the range of the drops in fugacity near the edges. Second, one would intuitively expect a low resistance for a membrane only one unit cell thick, because the atoms would be so hot upon entering and there would be little hindrance to their escape. This is why we decided to check for the effect. Finally, the long-range effect at the surfaces may reflect the rarity of gas−gas encounters inside the solid. Clearly, the absence of gas atoms at one end of the crystal would induce a flux, but gas atoms cannot determine such absence without encountering other gas atoms. A similar argument would apply in the case of a positive occupation gradient, as at the entrance. The rarity of gas encounters may stunt the dissipation of whatever surface effects exist.

3.3. Entrance and Exit Resistances. In the last part of this work, the entrance and exit of methane molecules have been studied independently to avoid any possible coupling effect. In these simulations CV II has been filled with crystal cells and adsorption or desorption steps have been simulated by setting inlet and outlet pressures. The "pressures" in the CVs interior to the crystal were determined by the pressure of the ideal gas being equilibrated in the GCMC sampling.

Entrance simulations combine the adsorption and intra-crystalline transport effects. The total resistance acting on this system is the sum of adsorption and intra-crystalline resistance:

$$R_{ads} = R_{tot} - R_{intra} = R_{tot} - \frac{L_{intra}}{D_{intra}} \qquad (20)$$

The pressures of CV I and CV II are set to 1 and 0 bar, respectively, to set the chemical potential gradient. The chemical potential gradient is then converted to fugacity gradient by relating the latter to $\exp(\beta\mu)$. Figure 6 shows a sudden drop in fugacity, thus in chemical potential, within the first 0.5 nm of the membrane that indicates the entrance resistance; the gradient further decreases linearly. The simulations show that for thinner crystals the adsorption resistance increases linearly with crystal

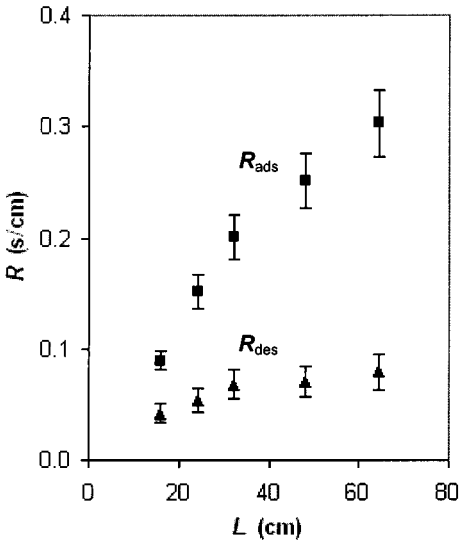

Figure 7. Change in individual resistance with increasing membrane thickness: Both adsorption and desorption indicate an approach to asymptotic values.

length, but when the thickness reaches $3L = 48$ nm, the resistance no longer appears to increase linearly, as shown in Figure 7.

Exit simulations combine the exit and intra-crystalline transport effects. The total resistance acting on this system is the sum of desorption ad intra-crystalline resistance:

$$R_{des} = R_{tot} - R_{intra} = R_{tot} - \frac{L_{intra}}{D_{intra}} \qquad (21)$$

In these simulations, CV I and CV II are set to 0 and 1 bar, respectively. Similar to entrance simulations, sudden drops in fugacity were observed within the first 0.5 nm of the membrane, indicating the exit resistance as shown in Figure 8. The increase of the desorption resistance is weaker compared to adsorption resistance and reaches its asymptotic value faster.

Results of the individual simulations for exit and entrance effects indicated that the resistance to adsorption is stronger than that to desorption. The magnitude of this difference increases with increasing crystal thickness but would presumably remain constant as the individual resistances approached their asymptotic values. When the sum of both resistances is

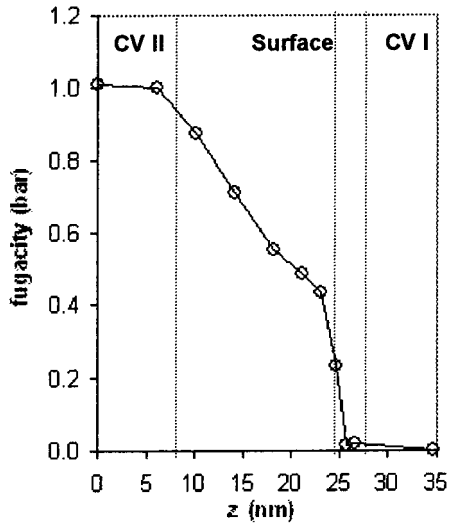

Figure 8. Fugacity gradient for the exit step: CV I and CV II are at vacuum and 1 bar, respectively.

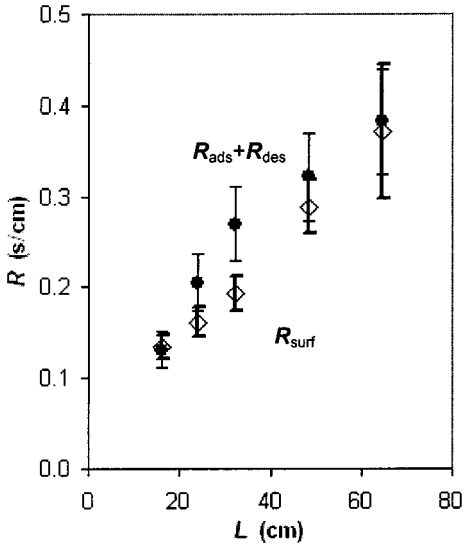

Figure 9. Comparison of surface resistances calculated from the membrane simulations and individual simulations.

compared with the total surface resistance, which has been calculated from the membrane simulations, it can be seen that they match within the error bars except for the 32 nm membrane (Figure 9). The discrepancy at 32 nm may result from underestimating the error bars at this condition, but the trend in the sum of individual resistances is concave down whereas the trend for the full membrane resistance is linear. Note that the full membrane includes both entrance and exit effects, however. Therefore the full membrane would need to be as thick as the desorption induction zone plus the adsorption induction zone before it would be expected to approach its asymptotic value. We can crudely estimate the thickness required for the total membrane resistance to plateau by assuming first-order responses for the two induction zones. In this manner, we estimate that adsorption reaches 90% of its plateau at 155 nm and desorption reaches 90% of its plateau value at 50 nm. Therefore, we estimate that the full membrane must be roughly 200 nm thick to exhibit its asymptotic behavior.

4. Conclusion

In this work we showed that the contribution of surface resistance to the overall transport resistance in zeolite membranes is larger and longer range than one might expect. A model is proposed on the basis of the additivity of corresponding mass-transfer resistances acting on entrance, intra-crystalline, and exit steps of the diffusion process. From the individual simulations of exit and entrance zones, it has been shown that the desorption resistance approaches an asymptote after roughly 50 nm of crystal thickness. The adsorption resistance, on the other hand, just begins to show an asymptotic trend within the maximum range of thickness feasible in the current study (64 nm). Extrapolating this trend indicates an asymptotic approach for membranes roughly 150 nm in thickness. However, the asymptotic trend has not been observed in full membrane simulations within the thickness limit of the work, possibly because of the coupling between the entrance and exit effects.

Since the surface resistance is limited to less than 1 μm and the single-crystal membrane comprises 100 μm, the surface resistance still represents a relatively small contribution to the overall resistance for this particular application. Thus, the diffusion process of pure components through the single-crystal membrane is dominated by the internal transport of the sorbate molecules along the principal axis of the crystal. Nevertheless, surface resistance may be more important in other applications such as pervaporation or polycrystalline membranes. For example, most of the pervaporation separation is expressed in the "skin" region, which ranges from 50 to 200 nm in thickness. Larger molecules might also exhibit slower approaches to steady state. We hope to study similar effects for ethane soon and for the competitive adsorption in mixtures.

Acknowledgment. This work was supported in part by the National Science Foundation. (Grant No. CTS-9725256)

References and Notes

(1) Karger, J.; Ruthven, D. M. *Zeolites* **1989**, *9*, 267−281.
(2) Ruthven, D. M. *Stud. Surf. Sci. Catal.* **1995**, *97*, 223−234.
(3) Sun, M. S.; Talu, O.; Shah, D. B. *AIChE J.* **1996**, *42*, 3001−3007.
(4) Talu, O.; Sun, M. A.; Shah, D. B. *AIChE J.* **1998**, *44*, 681−694.
(5) Kocirik, M.; Struve, P.; Fiedler, K.; Bulow, M. *J. Chem. Soc., Faraday Trans. 1* **1998**, *88*, 3001.
(6) Ford, D. M.; Glandt, E. D. *J. Membr. Sci.* **1995**, *107*, 47−57.
(7) Barrer, R. M. *Langmuir* **1987**, *3*, 309.
(8) Karger, J.; Ruthven, D. M. *Diffusion in Zeolites and Other Microporous Solids*; Wiley: New York, 1992.
(9) Maginn, E. J.; Snurr, R. Q.; Bell, A. T.; Theodorou, D. N. *Stud. Surf. Sci. Catal.* **1997**, *105*, 1851−1858.
(10) Heffelfinger, G. S.; van Swol, F. *J. Chem. Phys.* **1994**, *100*, 7548−7552.
(11) Nicholas, J. B.; Trow, F. R.; Mertz, J. E.; Hopfinger, A. *J. Phys. Chem.* **1993**, *97*, 4149−4163.
(12) Hernandez, E.; Catlow, C. R. A. *Proc. R. Soc. London Ser. A* **1995**, *448*, 143.
(13) Vingé-Maeder, F.; El Amrani, S.; Gélin, P. *J. Catal.* **1992**, *134*, 536−541.
(14) Arya, G.; Maginn, E. J.; Chang, H.-C. *J. Phys. Chem. B* **2001**, *105*, 2725.
(15) Takaba, H.; Koshita, R.; Muzkami, M. *J. Membr. Sci.* **1997**, *134*, 127−139.
(16) Martin, M. G.; Thompson, A. P.; Nenoff, T. M. *J. Chem. Phys.* **2001**, *114*, 7174−7181.
(17) Frenkel, D.; Smit, B. *Understanding Molecular Simulation: from Algorithms to Applications*; Academic Press: San Diego, 1996.
(18) Xu, L.; Tsotsis, T. T. S. M. *J. Chem. Phys.* **1999**, *111*, 3252−3264.
(19) Gaurav, A.; Chang, H.-C.; Maginn, E. J. *J. Chem. Phys.* **2001**, *115*, 8112−8124.
(20) Vlugt, T. J. H.; Krishna, R.; Smit, B. *J. Phys. Chem. B* **1999**, *103*, 1102−1118.
(21) Smit, B.; Siepmann, J. I. *J. Phys. Chem.* **1994**, *98*, 8442−8452.
(22) June, R. L.; Bell, A. T.; Theodorou, D. N. *J. Phys. Chem.* **1990**, *94*, 8232.
(23) Talu, O.; Myers, A. L. In *Fundamentals of Adsorption*; LeVan, M. D., Ed.; Kluwer: 1996; p 945.